Conference Proceedings Paper

High resolution historical topography: getting more from archival aerial photographs

Simone Seccaroni [1], Michele Santangelo [1,*], Ivan Marchesini [1], Alessandro C. Mondini [1] and Mauro Cardinali [1]

[1] Consiglio Nazionale delle Ricerche - Istituto di Ricerca per la Protezione Idrogeologica (CNR-IRPI). Via della Madonna Alta, 126 - 06128 Perugia, Italy
* Correspondence: michele.santangelo@irpi.cnr.it

Abstract: High resolution elevation data is a fundamental information for multiple applications in geomorphology spanning from visual analyses to modeling. Nowadays, gathering of high-quality elevation data relies on multiple sensors and technologies which can be mounted on terrestrial, aerial and satellite platforms. In the last years, the Structure from Motion (SfM) algorithms have made possible the acquisition of high and very-high resolution elevation data from optical images acquired with high overlapping rates at virtually no cost. Such a feature made it possible to exploit remote sensing archival imagery to build historical topographic information with unprecedented detail. However, despite the increasing number of applications of SfM algorithms in the scientific literature, still little has been done in terms optimization and quality evaluation of the results. We have applied the SfM algorithm developed in the photogrammetric open source software MicMac to six black and white aerial photographs taken in 1954 at 1:33.000 in a mountainous and steep area in Central Italy. The aim of the experiment consists in a quantitative evaluation of the digital surface models obtained for different scanning settings.

Keywords: aerial photographs; digital photogrammetry; open source; MicMac; high-resolution topography; GNSS

1. Introduction

Photogrammetry allows the reconstruction of the shape and metric of an investigated object, starting from measurements of points on photographs. The recent development of photogrammetric algorithms such as Structure from Motion (SfM) and multi-view-stereo (MVS) algorithms opens an unprecedented possibility to derive high-resolution Digital Surface Models (DSMs) from archival images despite the common lack of the calibration certificates [1–4].

Although the number of papers dealing with SfM algorithms in the scientific literature is increasing, more work still needs to be done to evaluate the quality of the resulting DSMs and to optimize the digitalization process [1,5]. In this work, we test how photographs digitalization settings (geometric and radiometric resolution) affect the accuracy of the output DSMs obtained applying the same photogrammetric processing chain. We processed six archival aerial photographs taken in 1954 at 1:30.000 scale in a mountainous and steep area in Central Italy, which topography represents a challenge for producing photogrammetric DSMs.

Both proprietary and open source photogrammetric software applications exist, which are used for work and research [6–8]. Unlike proprietary software, however, open source gives the possibility to examine [9,10], modify and redistribute the algorithms, and is particularly suitable for research reproducibility and replicability [11] and closer to the general concept of open science [12]. For this work, we have adopted MicMac, an open source photogrammetric software that implements SfM and and MVS algorithms [13].

2. Study area

The study area is a 35 km^2 wide area in the Northern Apennines, Central Italy. The area shows the common features of a mountainous region: elevation spans between 610 and 1560 m a.s.l., and the highest slope reaches 90°. Furthermore, due to the bedding attitude of the rocks that crop out in the study area, overhanging sandstone and limestone cliffs are a diffuse feature. The relative relief within the study area is particularly high. This is due to the presence of five major valleys which converge in the eastern part of the study area (Figure 1). Landcover is mainly wooded and scarcely built up, with few and sparse cultivated fields. Above 1.200 m a.s.l., landcover is mainly bare soil or grass.

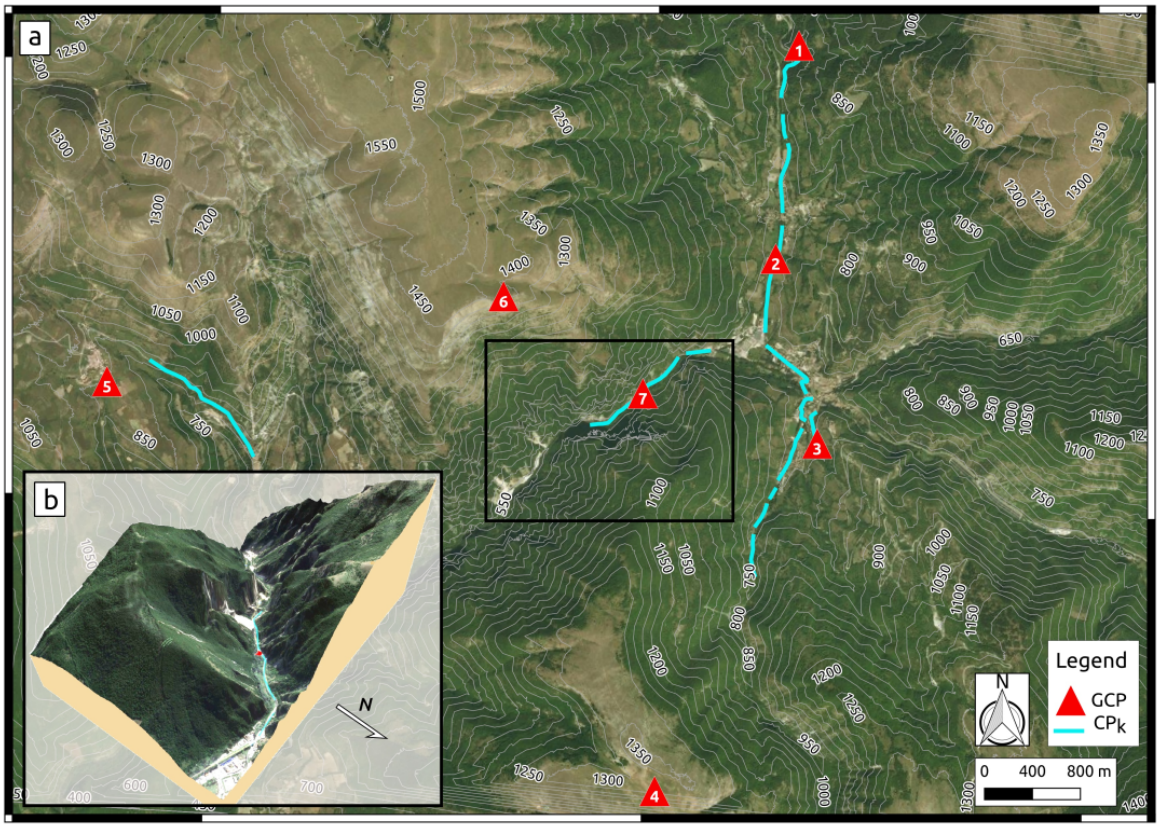

Figure 1. Study area. (**a**) Main map. Red triangles indicate the locations of the GCPs; blue lines indicate the path followed to collect control points in kinematic mode (CP_K). (**b**) Perspective view of the central portion of the study area.

3. Materials

The area of interest is covered by six black and white 23x23cm aerial photographs (printings of original negative films), acquired in September 1954 at approximately 1:33.000 scale with a calibrated focal length of 153.78mm, using a FAIRCHILD camera. The photographs belong to two strips, which have an overlap of 60% and a sidelap of 40%.

For the computation of the DSMs, we used an Asus G750JX laptop, with a Intel© Core^{TM} i7 4700HQ 8-cores processor, 24GB of DDR3 RAM memory and NVIDIA® GeForce® GTX 770M GPU graphic chip-set with 3GB DDR5 dedicated memory.

The digitalization of the aerial photographs was carried out by the Epson expression 10000 XL scanner. Its maximum geometric resolution is 2.400 dpi at a maximum of 16 bit in gray-scale and 32 bit in color mode.

The survey to collect ground control points (GCPs) and control points in kinematic mode was carried out using the GNSS receiver Leica Zeno 20, mounting the external antenna Leica AS10, and it was used in RTK mode, which allowed for a centimetric accuracy.

The software used at different steps of this work were: (i) SilverFast 6.6, (ii) MicMac [14].

4. Procedure to obtain the photogrammetric DSM

The first step of the procedure consisted in scanning the photographs. Each photograph was acquired at 400, 800, 1600 and 2400 dpi in gray-scale both at 8 and 16 bit using SilverFast software, for a total of 8 datasets. Images were then cropped using a rectangle mask, with the sides tangent to the fiducial marks.

In the second step, the images *exif* proprieties were edited (MicMac command *SetExif*) to provide information on focal length F_{mm} and equivalent focal length F_{35} for the internal calibration. The focal value was available from the distributor website (photograph example). The 35 mm equivalent focal length (F_{35}) was computed as follows: $F_{35} = F_{mm} * W_{35}/W_{film}$, where W_{35} is the film width (in millimeters) for a 35 mm camera, and W_{film} is the film width of the acquisition camera (in millimeters). In this case, F_{35} was equal to 23.86 mm.

The third step consists in the tie points definition (homologous pixels automatically detected across different images) through an image matching process performed by the MicMac tool *Tapioca*.

In the next step masks can be created to prevent MicMac from unnecessary computation. The graphical interface tool used is *SaisieMasqQT*. Then, tie-points are filtered out by *HomolFilterMasq*.

The bundle block adjustment (BBA) is performed in the fifth step by the MicMac command *Tapas*, an interface to the more complex tool *Apero* [15].

In the sixth step, GCPs have to be identified and selected on each image by a graphic interface (tool *SaisieAppuisInitQT*). The GCP ground absolute coordinates and the user-defined uncertainties are stored in a .txt file, then converted in a .xml file by the tool *GCPConvert*.

In the next step, a rigid transformation from the model coordinate system *Arbitrary* to the absolute coordinate system *GroundInt* is performed by the tool *GCPBascule*. Subsequently, a second BBA that fits tie points and GCPs is performed by the command *Campari* which calls the tool *Apero*.

Lastly, once the sparse point cloud has been generated, MicMac can proceed to the dense matching by the tool *Malt*. Finally, the dense point cloud is exported in .ply format by *Nuage2Ply*.

5. Ground Control Points

To further constrain the model, GCPs were collected by a GNSS survey. When collecting GCPs, care was taken to avoid cluster effects, and covering as homogeneously as possible the study area, also in elevation [16]. Particular attention was paid to the portion of the area covered by the black outlined rectangle in Figure 1. Due to the poorly built up landscape around the only municipality in the area (Visso) in 1954, and the difficulty in accurately finding the corresponding location of GCPs in today's landscape, most of the GCPs was selected at crossroads or on structures (Figure 1). For each of the 7 GCPs collected, longitude, latitude and elevation above ETM 2008 geoid were acquired using the available GNSS equipment in RTK mode. Elevation was converted to ITA 2005 geoid, more accurate for Italy.

To collect CPs for the DSMs validation, a GNSS survey was conducted in the field using the true kinematic method. The antenna was mounted on a car, and the frequency of acquisition set to 1 point every 10 meters. The over 1,000 points in the area were collected along two roads approximately running in the N-S and E-W directions (Figure 1). The points with uncertainties greater than 10 cm were filtered out, obtaining a robust set of elevation data used as control points (CP_K) to validate the output DSMs.

6. Results and discussion

Table 1 summarizes the results of the experiment presented. For reference, the first four rows describe the characteristics of the eight datasets.

When considering the number of tie points generated, no appreciable difference is observed across color depths. The highest number of tie points were obtained for 800 dpi (both 8 and 16 bit) images. Furthermore, a decreasing trend in BBA error is observed across scanning resolutions. However, the improvement between the 1600 and 2400 dpi datasets is negligible, both at 8 and 16 bit.

Table 1. Results for the 8 datasets. GSD, Ground Sampling Distance; BBA, Bundle Block Adjustment; P.E., Projection Error; GCP, Ground Control Point; DSM, Digital Surface Model; H-MAE, Mean Absolute Error of residuals in elevation; H-RMSE, Root Mean Square Error along elevation. Units of measure not belongin to the SI: *dpi*, dots per inch; *px*, pixels; p/m^2, points per square meter; *min*, minutes. Dataset names: 800g16 indicates an image scanned at 800 dpi, in gray-scale, and at 16 bit.

Dataset name	**400g8**	**800g8**	**1600g8**	**2400g8**	**400g16**	**800g16**	**1600g16**	**2400g16**
Scanned images								
Resolution [*dpi*]	400	800	1600	2400	400	800	1600	2400
Color depth [*bit*]	8	8	8	8	16	16	16	16
Pixel size [μm]	56	28	14	9	56	28	14	9
Approx. GSD [*m*]	1.91	0.95	0.48	0.32	1.91	0.95	0.48	0.32
Sparse point cloud								
Tie points [*thousands*]	62.1	79.9	75.4	66.6	62.4	79.7	75.4	66.8
BBA P.E. [*px*]	0.32	0.459	0.71	0.981	0.319	0.469	0.725	0.981
BBA & GCP, P.E. [*px*]	0.363	0.512	0.683	0.949	0.362	0.537	0.789	0.948
BBA & GCP, P.E. [*m*]	0.69	0.49	0.33	0.3	0.69	0.51	0.38	0.3
Dense point cloud								
Mean density [p/m^2]	0.33	1.33	5.31	11.74	0.33	1.33	5.3	11.77
DSM								
DSM Resolution [*m*]	2	1	0.5	0.35	2	1	0.5	0.35
Computation time								
Tapioca [*min*]	6	21	30	40	6	22	28	40
Malt [*min*]	23	87	449	1294	19	84	430	1175
Internal coherence								
3D MAE [*m*]	0.27	0.11	0.20	0.27	0.36	0.16	0.23	0.27
3D RMSE [*m*]	0.50	0.16	0.28	0.40	0.59	0.20	0.40	0.40
Model validation								
Mean [*m*]	-0.81	-0.2	-1.08	-0.89	-1.01	-0.21	-1.18	-0.94
Median [*m*]	-0.48	-0.36	-0.92	-0.77	-0.48	-0.36	-0.92	-0.77
Standard dev. [*m*]	2.51	2.11	1.66	1.79	2.65	1.97	1.7	1.85
H-MAE [*m*]	1.96	1.66	1.52	1.54	2.06	1.54	1.6	1.58
H-RMSE [*m*]	2.64	2.11	1.98	2	2.84	1.97	2.07	2.07

Table 1 also reports the running time of *Tapioca* and *Malt*, the most demanding (parallelized) tools of the entire pipeline. The time increase trend is steeper for *Malt* compared to *Tapioca*. Therefore, processing images at high geometric resolutions implies more time expense due to the dense matching process. On the other hand, it is observed that increasing the radiometric resolution does not lead to running time increase, neither for *Tapioca*, nor for *Malt*.

The distance between the seven GCPs and the location of the same GCPs computed by the model [13] can be considered as an indicator of its internal coherence. In detail, Table 1 shows the two indicators MAE and RMSE. Inspection of Table 1 reveals that (i) g8 datasets have residuals comparable to or slightly smaller than the corresponding g16 datasets, (ii) the 800g8 dataset shows the lowest residuals, (iii) the minimum values of RMSE and MAE were obtained for 800 dpi (both for 16 bit and 8 bit scanned images). Unexpectedly, we notice that increasing color depth does not necessarily correspond to an increased internal coherence. We hypothesize that this can be due to

the fact that the original images are grey-scale printed photographs. Since previous research indicate that 16 bit acquisition is advised as a best practice [17], based on our results, further tests should be carried out to further look into this topic.

The total 8 dense point clouds were projected into DSMs, which resolution was set close to the GSD of the starting images (Table 1).

To evaluate the accuracy of the eight DSMs, we computed the difference between the elevation of each CP_K and the elevation of each DSM at the planimetric location of each CP_K. Outliers were singled out and filtered according to a three-sigma ($3\,\sigma$) error criterion. Statistics of residuals distributions is shown in the last section of Table 1.

Inspection of model validation data (Table 1) shows that 800g8 is the best dataset in terms of mean value proximity to zero, which can be taken as indicator of small systematic error. Anyway, as already mentioned above, 1600g8 has the smallest standard deviation, which can be taken as indicator of good relative accuracy. Moreover, 1600g8 has the smallest root mean squared error (RMSE), which takes into account both random and systematic error [18]. Finally, 1600g8 has also the smallest mean absolute error (MAE), which is an even more important quality indicator than RMSE, according to some authors [19]. To check for normality of the two best distribution candidates 800g8 and 1600g8, we made a one-sample Kolmogorov-Smirnov test. The 800g8 dataset seems better normally distributed, showing a maximum distance value of 0.20 compared to the 0.30 of the 1600g8 dataset.

Overall, considering the model internal coherence, the mean point density of the point clouds, and the results of the model validation (Table 1), it emerges that the optimal performance was obtained at 1600 dpi for images scanned at 8 bit, whereas it was obtained at 800 dpi for images scanned at 16 bit. When compared to the computation time, it is also clear that a low increase in the internal model of 2400 dpi (8 and 16 bit) corresponds to a computation time way too large compared to the 1600 dpi datasets. Such an evidence underlines that acquisition at 2400 dpi appears inconvenient, even for high-performance machines. Moreover, Table 1 shows that the number of tie points automatically detected by *Tapioca* decreases with the increasing scanning resolution higher than 800 dpi.

7. Conclusions

This work quantified the influence of acquisition of archive aerial images on the accuracy of DSMs produced applying photogrammetric algorithms, and hence can help to define the best acquisition mode to get the most from archival aerial photographs.

Limitedly to the historical aerial photographs used in this study (available for the entire Italian territory), results revealed that the optimal scanning geometrical resolution is between 800 and 1600 dpi, and that the radiometric resolution does neither affect computation time nor provide any quality improvement of the final DSMs.

The photographs used in this experiment belong to an extensive aerial photographic survey conducted between 1954 and 1956 over all the Italian territory. Based on this study, such large set of historical aerial photographs can be exploited to produce DSMs at a resolution between 0.5 and 1 m with errors close to 2 m in elevation. Such an invaluable dataset could provide accurate high-resolution quantitative information on topography, which is of great value for multiple studies in Earth Science.

Author Contributions: S.S. performed the analysis and field surveys, I.M and M.S. conceived and designed the experiments, wrote the paper and analyzed the data; M.C. and A.C.M. contributed materials and revised the manuscript

Bibliography

1. Godone, D.; Garbarino, M.; Sibona, E.; Garnero, G.; Godone, F. Fotogrammi storici, uno strumento per rappresentare l'italia che cambia. *Bollettino dell'Associazione Italiana di Cartografia* **2011**.

2. Pulighe, G. Ortorettifica di foto e aree storiche per lo studio delle dinamiche ambientali in regioni montane. *GEOmedia* **2009**, *13*.
3. Nocerino, E.; Remondino, F. Uso consapevole di software speditivi per la ricostruzione 3D. *GEOmedia* **2016**, *20*.
4. Remondino, F.; Pizzo, S.D.; Kersten, T.P.; Troisi, S. Low-Cost and Open-Source Solutions for Automated Image Orientation – A Critical Overview. Progress in Cultural Heritage Preservation. Springer, Berlin, Heidelberg, 2012, Lecture Notes in Computer Science, pp. 40–54.
5. Mertes, J.R.; Gulley, J.D.; Benn, D.I.; Thompson, S.S.; Nicholson, L.I. Using structure-from-motion to create glacier DEMs and orthoimagery from historical terrestrial and oblique aerial imagery. *Earth Surface Processes and Landforms* **2017**, *42*, 2350–2364.
6. Jaud, M.; Passot, S.; Le Bivic, R.; Delacourt, C.; Grandjean, P.; Le Dantec, N. Assessing the Accuracy of High Resolution Digital Surface Models Computed by PhotoScan® and MicMac® in Sub-Optimal Survey Conditions. *Remote Sensing* **2016**, *8*, 465.
7. Duarte, L.; Teodoro, A.C.; Moutinho, O.; Gonçalves, J.A. Open-source GIS application for UAV photogrammetry based on MicMac. *International Journal of Remote Sensing* **2017**, *38*, 3181–3202.
8. Benassi, F.; Dall'Asta, E.; Diotri, F.; Forlani, G.; Morra di Cella, U.; Roncella, R.; Santise, M. Testing Accuracy and Repeatability of UAV Blocks Oriented with GNSS-Supported Aerial Triangulation. *Remote Sensing* **2017**, *9*.
9. Remondino, F.; Spera, M.G.; Nocerino, E.; Menna, F.; Nex, F.; Gonizzi-Barsanti, S. Dense image matching: Comparisons and analyses. 2013 Digital Heritage International Congress (DigitalHeritage), 2013, Vol. 1, pp. 47–54.
10. Bakker, M.; Lane, S.N. Structure from Motion (SfM) photogrammetry applied to historical imagery: plug & play? 2017, Vol. 19, p. 10446.
11. Ince, D.C.; Hatton, L.; Graham-Cumming, J. The case for open computer programs. *Nature* **2012**, *482*, 485.
12. Minelli, A.; Oggioni, A.; Pugnetti, A.; Sarretta, A.; Bastianini, M.; Bergami, C.; Aubry, F.B.; Camatti, E.; Scovacricchi, T.; Socal, G. The project EcoNAOS: vision and practice towards an open approach in the Northern Adriatic Sea ecological observatory. *Research Ideas and Outcomes* **2018**, *4*, e24224, [https://doi.org/10.3897/rio.4.e24224].
13. Mölg, N.; Bolch, T. Structure-from-Motion Using Historical Aerial Images to Analyse Changes in Glacier Surface Elevation. *Remote Sensing* **2017**, *9*.
14. Rupnik, E.; Daakir, M.; Pierrot Deseilligny, M. MicMac – a free, open-source solution for photogrammetry. *Open Geospatial Data, Software and Standards* **2017**, *2*, 14.
15. Deseilligny, M.P.; Cléry, I. Apero, an open source bundle adjusment software for automatic calibration and orientation of set of images. Proceedings of the ISPRS Symposium, 3DARCH11, 2011, Vol. 269277.
16. Santangelo, M.; Marchesini, I.; Bucci, F.; Cardinali, M.; Fiorucci, F.; Guzzetti, F. An approach to reduce mapping errors in the production of landslide inventory maps. *Natural Hazards and Earth System Sciences* **2015**, *15*, 2111–2126.
17. Nocerino, E.; Menna, F.; Menna, F. Multi-temporal analysis of landscapes and urban areas. *ISPRS - International Archives of the Photogrammetry, Remote Sensing and Spatial Information Sciences* **2012**, *XXXIX-B4*, 85–90.
18. Pulighe, G.; Fava, F. DEM extraction from archive aerial photos: accuracy assessment in areas of complex topography. *European Journal of Remote Sensing* **2013**, *46*, 363–378.
19. Pontius, R.G.; Thontteh, O.; Chen, H. Components of information for multiple resolution comparison between maps that share a real variable. *Environmental and Ecological Statistics* **2008**, *15*, 111–142.